Low and high intensity velocity selective coherent population trapping in a two-level system

David Wilkowski, Maryvonne Chalony, Robin Kaiser, Anders Kastberg

Low and high intensity velocity selective coherent population trapping in a two-level system

D. Wilkowski[1], M. Chalony[1], R. Kaiser[1] and A. Kastberg[2]

[1] *Institut Non Linéaire de Nice - CNRS, UMR 6618, University de Nice Sophia-Antipolis, F-06560 Valbonne, France*
[2] *Umeå University - Department of physics, SE-90187 Umeå, Sweden*

PACS 37.10.De – Atom cooling methods
PACS 37.10.Vz – Mechanical effects of light on atoms, molecules, and ions

Abstract. - An experimental investigation is made of sub-recoil cooling by velocity selective coherent population trapping in a two-level system in Sr. The experiment is carried out using the narrow linewidth intercombination line at 689 nm. Here, the ratio between the recoil shift and the linewidth is as high as 0.64. We show that, on top of a broader momentum profile, subrecoil features develop, whose amplitude is strongly dependent on the detuning from resonance. We attribute this structure to a velocity selective coherent population trapping mechanism. We also show that the population trapping phenomenon leads to complex momentum profiles in the case of highly saturated transitions, displaying a multitude of subrecoil features at integer multiples of the recoil momentum.

Introduction. – The role of quantum interference in atomic physic has been demonstrated in several impressive experiments, *e.g.*, in [1–3]. Already in the 1970'ies, it was shown that quantum interference can prevent absorption in the presence of resonant light [4]. Indeed, if considering a Λ-shape configuration of internal states (two ground states and one excited state), there will exist a coherent superposition of the two ground states, for which the two excitation amplitudes to the excited state interfere destructively. For counter propagating laser beams, such a dark state is velocity sensitive, and it can thus be used for cooling processes going below the single photon recoil energy. An experimental proof of such 'velocity selective coherent population trapping' (VSCPT) was first demonstrated in one dimension in 1988 [5]. The experimental signature consisted of two peaks in the momentum distribution, centred at the momenta $\pm\hbar k$, and of sub-recoil widths. A few years later, VSCPT was also observed in 2D and 3D [6, 7]. Those experiments were done on the $J_g = 1 \rightarrow J_e = 1$ transition in metastable helium at 1.08 μm, using a near resonant laser with $\sigma^+ - \sigma^-$–polarisation configuration. Hence, two major requirements for VSCPT were fulfilled: firstly, the existence of a closed family of states with respect to the laser interaction; secondly the resulting dark state is also an eigenstate of the kinetic energy Hamiltonian. Thus, the dark state gets an infinitely long lifetime leading to arbitrary narrow peaks in the momentum distribution. In such conditions, very low temperatures have been obtained [8].

For transitions with higher angular momenta than in the above mentioned He*-experiments (*i.e.*, with ground state angular momentum quantum numbers $J_g \geq 2$), at least one dark state exists if ($J_e = J_g$) or ($J_e = J_g - 1$). However those dark states are not eigenstates of the kinetic Hamiltonian. In reference [9], the authors suggest to add an extra off-resonant laser beam to induce light shifts in order to exactly compensate the kinetic energy mismatch. Without any compensation, the dark state acquires a finite lifetime due to motional coupling. As far as the lifetime of this state remains long with respect to other states, it can be favoured by the system [10]. Thus it may be possible to observe VSCPT with sub-recoil peaks at momenta $\pm M_J\hbar k$ with $M_J \geq 1$, where M_J is the magnetic quantum number describing the projection of J_g. So far no experimental data have been published using such a configuration. High momentum dark states has been reported for the case with a $J_g = 1 \rightarrow J_e = 1$ transition in metastable helium using a lin-angle-lin polarisation configuration [11]. In that case, the dark states are characterised by two peaks at momenta $\pm Q\hbar k$, where Q is an integer. Thus, the high momentum states are still eigenstates of the kinetic Hamiltonian.

From reference [10], we learn that observed momentum states are not necessarily totally dark states, and are thus

not eigenstates of the total atom–laser Hamiltonian. However they should be the most protected states with respect to spontaneous emission processes. Following this idea and reference [11], the requirement of a closed family for VSCPT does not have to be strictly fulfilled. Indeed, considering a two-level atom coupled with a nearly resonant laser, the coherent superposition of ground states with different momenta;

$$\frac{1}{\sqrt{2}}\left(|\mathrm{g}\,;-\hbar k\rangle - |\mathrm{g}\,;+\hbar k\rangle\right) \tag{1}$$

is not coupled to the excited state $|\mathrm{e}\,;0\rangle$. However the three involved states, do not form a closed family because of the coupling to the states $|\mathrm{e}\,;\pm 2\hbar k\rangle$. With a broad transition, *i.e.*, $\varepsilon = \omega_\mathrm{r}/\Gamma \ll 1$ (where Γ is the natural linewidth of the transition and $\omega_\mathrm{r} = \hbar k^2/2m$ is the recoil angular frequency), the coupling is not sensitive to a kinetic energy mismatch between the $|\mathrm{e}\,;0\rangle$ and $|\mathrm{e}\,;\pm 2\hbar k\rangle$ states and VSCPT will not occur. If, however $\varepsilon \approx 1$ (or even $\varepsilon \gg 1$), the unwanted transitions may be off-resonant, and the coherent superposition in equation 1 acquire a long lifetime. This situation, leading to VSCPT, has been numerically studied in [12] and was observed on a helium beam, with $\varepsilon = 0.22$ [13].

In this letter we report on observed VSCPT on the $^1\mathrm{S}_0 \rightarrow {}^3\mathrm{P}_1$ intercombination line in Sr at 689 nm. Here $\varepsilon = 0.64$ (with $\Gamma = 2\pi \times 7.5$ kHz). This more favorable value than the one used in [13] allows for a more pronounced observation of VSCPT in a two-level system at low intensity. The momentum distribution is still dominated by Doppler cooling effects, but an enhanced population builds up at the momenta $\pm\hbar k$. The amplitudes of these peaks strongly depend on the atom-laser detuning. Moreover, for a higher saturation parameter, multiple peaks in the momentum distribution are observed. This structure is not linked to any closed family of states and, in contrast to the low saturation case, does not correspond to an eigenstate of the kinetic Hamiltonian.

Experimental set-up. – The details of the experimental set-up, including two-stage cooling and trapping of Sr, can be found in [14, 15]. Briefly, the strontium atoms are first accumulated and cooled in a ('blue') magneto-optical trap (MOT) on the $\left(^1\mathrm{S}_0 \rightarrow {}^1\mathrm{P}_1\right)$ transition at 461 nm, and are then transferred into another ('red') MOT, running on the $\left(^1\mathrm{S}_0 \rightarrow {}^3\mathrm{P}_1\right)$ intercombination line at 689 nm, and with saturation intensity $I_\mathrm{sat} = 3\ \mu\mathrm{W/cm}^2$. The cold sample, with a 50 μm rms radius, contains about 10^6 atoms at a temperature of 1 μK. After the MOT phases, the atoms interact with an intensity balanced 1D standing wave along a horizontal direction. A 0.1 mT vertical magnetic bias field is applied in order to properly define the quantisation axis. This allows us to restrict the description of the dynamics to two atomic levels. The polarisation of the counter propagating laser beams is adjusted to be parallel to the magnetic field axis. A typical duration of the 1D optical molasses phase is between 0.5 ms and 2 ms. The interaction time is then always longer than the typical lifetime of the relevant internal states. Hence, the studies of the VSCPT cooling mechanism in this article are made in the steady state regime. However, this may not be the case for particular momentum distributions, where a steady state does not exist even for red frequency detuned laser [16].

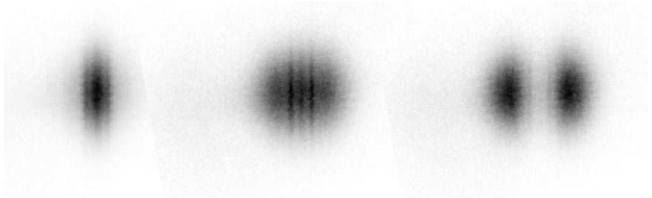

Fig. 1: Examples of time of flight images. The 1D optical molasses laser beams are along the horizontal axis in the figure, as well as in the experiment. From left to right, the angular detunings are $\delta = -3.1\omega_\mathrm{r}$, $-1.8\omega_\mathrm{r}$, and $-0.4\omega_\mathrm{r}$, and the intensities are $I = 5I_\mathrm{sat}$ for all images, where I_sat is the saturation intensity.

The momentum distribution is extracted this distribution using a time-of-flight (TOF) technique. The typical dark period of the TOF is 50 ms. Thereafter, a resonant probe at 461 nm is switched on for 40 μs, and the fluorescence signal is collected on an intensified CCD camera. The momentum resolution is limited by the finite size of the cloud after the 1D optical molasses phase. If this phase is not too long, the typical rms radius of the cold cloud is still about 50 μm, which leads to a momentum resolution of $\hbar k/6$. Images for background substraction are taken with the same procedure, but with no atoms in the blue and the red MOTs.

Experimental results. – In figure 1, we show examples of acquired TOF-images for three different detunings, but for otherwise identical laser parameters. The standing wave axis corresponds to the horizontal axis of the picture. By integrating along the vertical axis in fig. 1, we obtain more precise data for the momentum distributions. In figure 2, we show such momentum distributions for a range of detunings.

It is known that Doppler cooling on broad transitions ($\varepsilon \ll 1$) leads to Gaussian momentum distributions. In the present case, one can clearly see the more complex distribution resulting from Doppler cooling on narrow transitions. For instance we have observed that the minimum momentum dispersion is obtained at a detuning of about $\delta = -4\omega_\mathrm{r}$, in contrast to the case of broad transitions, where the minimum dispersion occurs at $\delta = -0.5\Gamma$, *i.e.*, $\delta \simeq -0.3\omega_\mathrm{r}$ (for $\varepsilon = 0.64$) [16]. For a detuning of $\delta = -0.5\Gamma$, laser cooling on a narrow transition yields to two separated maxima, a 'double hump': the atoms are expelled from the central region. This type of distribution is in qualitative agreement with the predicted non-stationary distribution reported in [16].

On the overall momentum distribution attributed to

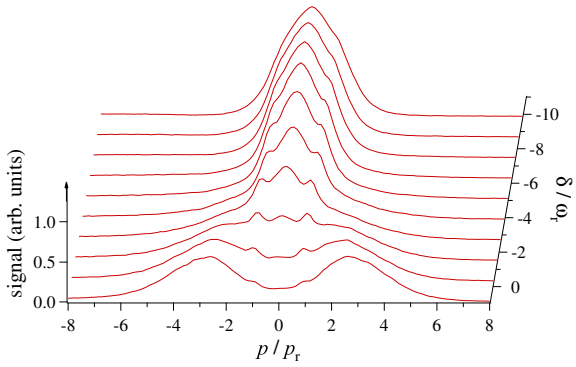

Fig. 2: Momentum distributions for the intensity $I = 5\,I_{\rm sat}$, and for angular detunings from $+0.9\,\omega_{\rm r}$ to $-11.1\,\omega_{\rm r}$. These profiles are directly obtained from images as in fig. 1, by integrating the image density along the vertical axis, and plotting against the horizontal axis. The latter is converted to momentum units, taking into account the TOF expansion time.

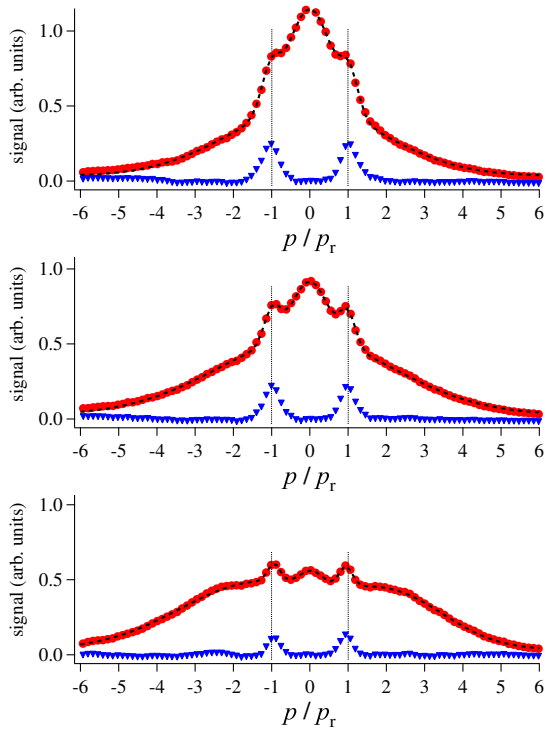

Fig. 3: Momentum profiles from fig. 2, for the angular detunings (from top to bottom), $-4.4\omega_{\rm r}$, $-3.1\omega_{\rm r}$, and $-1.8\omega_{\rm r}$. The raw data is the red circles. Fits to four Gaussians (five in the lowermost case), are presented by a dashed black line. The blue triangles are the raw data, subtracted by the resulting fit function, with exception of the two Gaussians that appear close to $\pm p_{\rm r}$. Thus, this is a good indication of the part of the atomic population that is in the semi-dark state. Vertical lines at $\pm p_{\rm r}$ are added, as a guide to the eye.

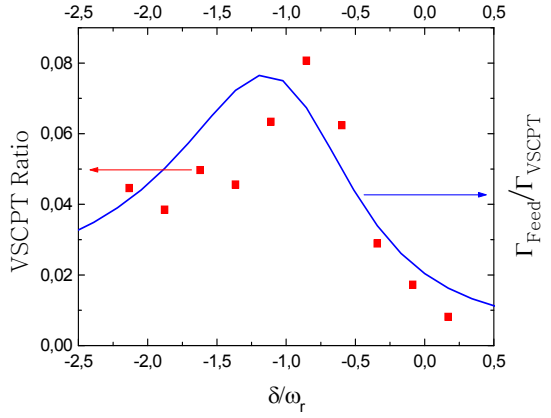

Fig. 4: Red squares: ratio of the atomic population in the VSCPT state, as a function of angular detuning. Blue line: ratio of the VSCPT feeding rate $\Gamma_{\rm Feed}$ and the VSCPT lifetime $\Gamma_{\rm VSCPT}$.

Doppler cooling are superimposed two sub-recoil peaks at $\pm\hbar k$ due to VSCPT [12]. The entire momentum distribution is described as a number of Gaussians. Two of those, centered at $p = \pm p_{\rm r}$, are used to account for VSCPT. In figure 3, we show such fits, corresponding to three of the traces in fig. 2. The figures also show the residuals from fits including only the broad Doppler features. The widths of the subrecoil VSCPT features are limited by the convolution with the initial size of the cloud, and we can thus not extract relevant information about the VSCPT velocity distribution. However, by integrating the VSCPT-peaks, we get a measure of the fraction of the population that is in the long lived (VSCPT) state. In figure 4 we show the fraction of atoms in the VSCPT-state as a function of detuning. This quantity remains relatively small, within the few percent range, and peaks around $-\omega_{\rm r}$ below the atomic resonance.

For higher laser intensity, the momentum distribution becomes more complex. An increasing number of subrecoil peaks, at momenta $\pm n\hbar k$ ($n \geq 1$) are now observed, as shown in figure 5. As we will discuss in the next section, these subrecoil structures can also be attributed to a VSCPT mechanism. Those peaks are even less pronounced and broader than for the low intensity case and a quantitative description is not easy to achieve. It is however important to note than the population fractions in the peaks are not necessarily the same or monotonously decreasing with momentum for a given experimental realisation. For example figure 6 clearly shows more pronounced peaks for the $p = 0, \pm 2\hbar k$ impulsion than for $p = \pm\hbar k$. We show in the following section that a long lived state appearing at high intensity can be attributed to the peaks at $p = 0, \pm 2\hbar k$.

Theoretical model and comparison with experiment. –

Effective Hamiltonian. A straightforward method to reveal the existence of long lived states is to diagonalize

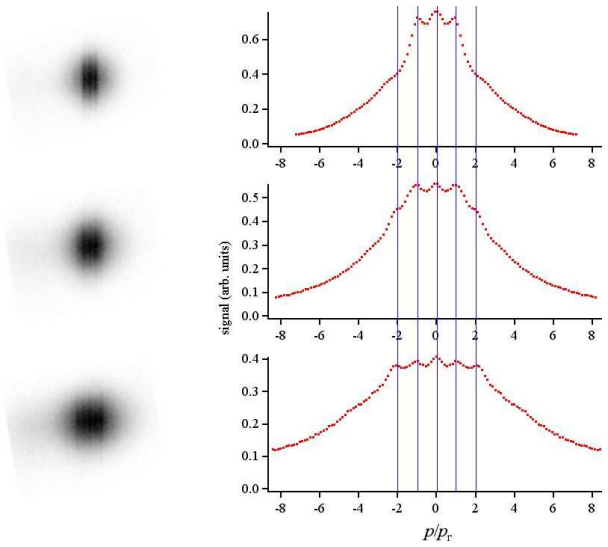

Fig. 5: Time of flight images and momentum distributions for high intensity. From top to bottom, the intensities are $I = 30I_{\rm sat}$, $130\,I_{\rm sat}$, and $350\,I_{\rm sat}$ with $\delta \simeq -5\omega_{\rm r}$. In the momentum distribution, vertical lines have been drawn at integer values of $p/p_{\rm r}$.

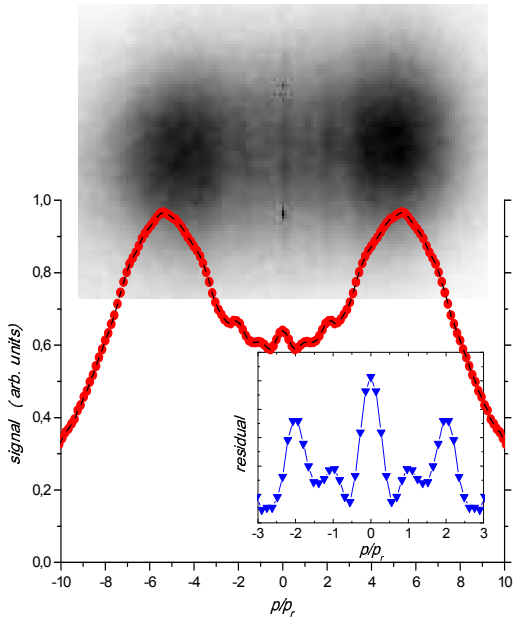

Fig. 6: Time of flight image at $I = 130I_{\rm sat}$ and $\delta = -2\omega_{\rm r}$, and the corresponding momentum distribution. To improve the signal-to-noise ratio the profile is symmetrized with respect to the center of the distribution. The insert shows a residual, where the slowly varying Doppler distribution has been removed.

the effective Hamiltonian, which takes into account the finite lifetime of the excited state [12]. In the rotating-wave approximation, it takes the following form:

$$\begin{aligned} H_{\rm eff} &= \frac{p^2}{2m} - \hbar\,(\delta + i\Gamma)\,|{\rm e}\,;p\rangle\langle {\rm e}\,;p| \\ &+ \frac{\hbar\Omega}{2}\left(|{\rm e}\,;p\rangle\langle {\rm g}\,;p+\hbar k| + |{\rm e}\,;p\rangle\langle {\rm g}\,;p-\hbar k|\right) . \quad (2) \end{aligned}$$

Here Ω is the Rabi frequency of the atom laser coupling and we have $\frac{2\Omega^2}{\Gamma^2} = \frac{I}{I_{\rm sat}} = s_0$, where I is the laser intensity and s_0 the resonant saturation parameter. The coupling term in the Hamiltonian only connects ground and excited states that have momentum differences of $\hbar k$. For this reason, one can reformulate the effective Hamiltonian in the following way:

$$\begin{aligned} H_{\rm eff} &= \sum_{n=-\infty}^{\infty}\left[\left(\frac{(q+2n\hbar k)^2}{2m} - \hbar\,(\delta + {\rm i}\Gamma)\right)\right. \\ &\times\ |{\rm e}\,;q+n\hbar k\rangle\,\langle {\rm e}\,;q+n\hbar k| \\ &+\ \frac{(q+2n\hbar k)^2}{2m}\,|{\rm g}\,;q+n\hbar k\rangle\,\langle {\rm g}\,;q+n\hbar k| \\ &+\ \frac{\hbar\Omega}{2}\,(\,|{\rm e}\,;q+n\hbar k\rangle\,\langle {\rm g}\,;q+(n+1)\hbar k| \\ &+\ \left.|{\rm e}\,;q+n\hbar k\rangle\,\langle {\rm g}\,;q+(n-1)\hbar k|\,)\,\right]\,, \qquad (3) \end{aligned}$$

with n being an integer and $0 \le q < \hbar k$. Each family of states is characterized by a q value and by an odd (resp. even) value of n for the ground state and an even (resp. odd) value of n for the excited state.

Strictly speaking, each family contains an infinite number of members. However, one can remove high-momentum states, since the Doppler shift brings them far off-resonance. Hence to solve the eigenstate equation, we choose $n_{\rm max}$, a maximum value of n, such that the coupling between the $|{\rm g(e)}\,;q \pm (n_{\rm max}-1)\hbar k\rangle$ state and the $|{\rm e(g)}\,;q \pm n_{\rm max}\hbar k\rangle$ state is small and has any impact on the eigenstates of interest. In figs. 7a and 7b, we show the real and the imaginary parts of the eigenvalues, corresponding to some of the eigenstates of the effective Hamiltonian (equation 3) for $\varepsilon = 0.64$ with $n_{\rm max} = 8$ and $q = 0$, as a function of the Rabi frequency.

Low intensity case. At low Rabi frequency, an expected behaviour corresponding to VSCPT on a two level system is observed. The VSCPT state, namely the long lived state, has an eigenvalue which corresponds to the red line (full line in figure 7b). Indeed, its imaginary part remains small when Ω increases, while its real part does not change significantly. At vanishing Ω, we check that the eigenstate is, as expected, the one defined by expression (1). The smooth dependency of the VSCPT state lifetime is mainly due to the off-resonant coupling to the $|{\rm e};2\pm\hbar k\rangle$ states. Thus one has

$$\Gamma_{\rm VSCPT} \xrightarrow[\Omega\to 0]{} \Gamma_{\rm off} = \frac{\Gamma\Omega^2}{\Gamma^2 + 4(\delta - 3\omega_{\rm r})^2}, \qquad (4)$$

where $\Gamma_{\rm off}$ is the red dashed line in figure 7b. On the other hand, the green line (in bold in figure 7b) corresponds to the coupling state orthogonal to the VSCPT state for vanishing Ω. At resonance, the lifetime $\Gamma_{\rm C}$ of this state is

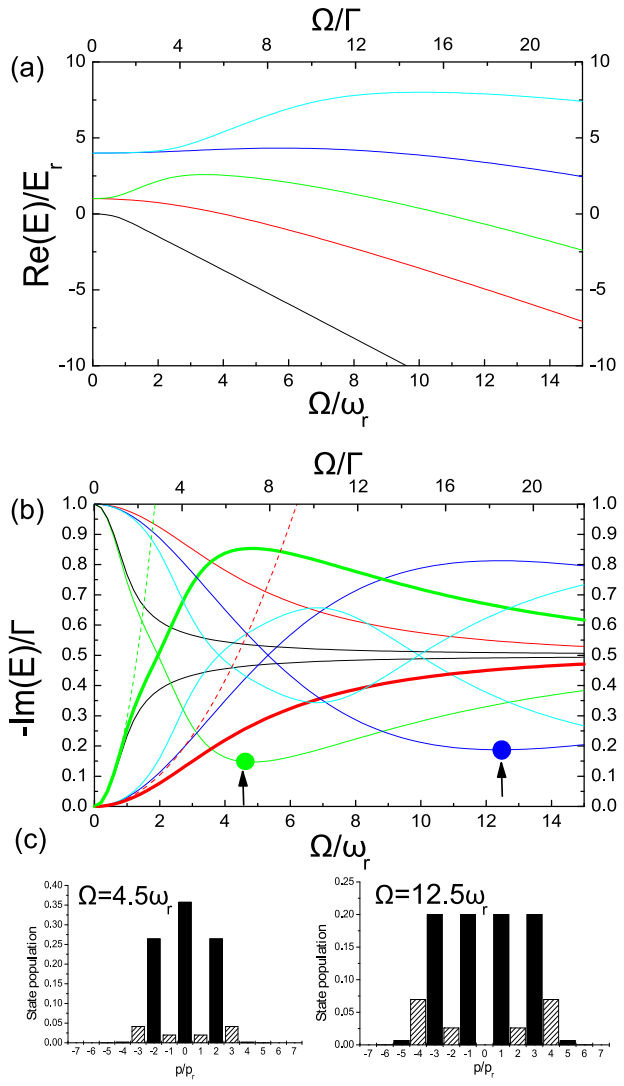

Fig. 7: Real (a) and imaginary parts (solid lines) (b) of the eigenvalues of the effective Hamiltonian given by the expression 3, with $n_{\max} = 8$ and $q = 0$, as a function of Ω. Only the eigenvalues corresponding to eigenstates for which the momentum $|p| \leq 2\hbar k$ at $\Omega = 0$ are shown. In (b) the dashed red and black lines correspond respectively to $\Gamma_{\rm off}$ and $\Gamma'(\delta+\omega_{\rm r})$, whereas the dash-dotted line corresponds to $\Gamma_{\rm C}$ in units of Γ (see text). At $\Omega \approx 4.5\omega_{\rm r}$ and $\Omega \approx 12.5\omega_{\rm r}$ long lived states appear, pointed out by arrows and coloured circles. The histograms in (c) represent the populations of the relevant momentum states in the ground state (plain bars) and in the excited state (dashed bars).

mainly due to the coupling to the $|{\rm e};0\rangle$ state:

$$\Gamma_{\rm C} \xrightarrow[\Omega\to 0]{} \Gamma_{\rm on} = \frac{\Gamma\Omega^2}{\Gamma^2 + 4(\delta+\omega_{\rm r})^2}. \qquad (5)$$

Indeed $\Gamma_{\rm on}$, which corresponds to the dashed green line in figure 7b, coincides with the green line at small Ω.

One can estimate the population of the VSCPT state by a simple feed and loss mechanism. One then assumes that the population is proportional to the ratio $\Gamma_{\rm feed}/\Gamma_{\rm VSCPT}$, where $\Gamma_{\rm feed} \approx (\Gamma_{\rm VSCPT} + \Gamma_{\rm C})/2$ is the feeding rate. Using the result given by the numerical simulation for evaluating $\Gamma_{\rm feed}/\Gamma_{\rm VSCPT}$, we compare this ratio to the experimental data points in figure 4. The result is very satisfactory.

High intensity case. If the two-level atom can be treated semi-classically, like for a broad transition for example, the two imaginary parts monotonously converge at high intensity to the same value, namely $\mathrm{Im}[E] = -\Gamma/2$. In the full quantum problem, similar behaviours are also observed. This is for example the case for the states $|e;p=0\rangle$ and $|g;p=0\rangle$ (black curves in figure 7b). In contrast, other states have unexpected non-monotonous behaviours. Some of them exhibit minima as a function of Ω, sort as the one depicted by a *green* line at $\Omega \approx 4.5\omega_{\rm r}$ and a *blue* one at $\Omega \approx 12.5\omega_{\rm r}$. Those states are of particular interest as they are long lived ones. We will now demonstrate that those states are at the origin of the multi peak structures experimentally observed at high intensity.

Figure 7c shows the normalized population of the momentum states, for the two long lived state. If a two-peak structure at $p = \pm\hbar k$ is a characteristic of VSCPT at low intensity, an increasing number of peaks is predicted by our model and also observed in the experiment at higher intensity. For example the long lived state at $\Omega \approx 4.5\omega_{\rm r}$ is mainly composed of three peaks, at $p = 0$ and at $p = \pm 2\hbar k$. At $\Omega \approx 12.5\omega_{\rm r}$ a four-peak structure at $p = \pm\hbar k$ and $p = 3 \pm \hbar k$ is expected.

Lets focus on the simplest case, namely the three peak case at $\Omega \approx 4.5\,\omega_{\rm r}$, and derive an analytical expression for the state lifetime. In the view of the most abundant peak population, we restrict ourselves to $n_{\max} = 2$ and consider only the closed family $\{|{\rm g}\,;q\rangle\,, |{\rm e}\,;q \pm \hbar k\rangle\,, |{\rm g}, q \pm 2\hbar k\rangle\}$. Under this condition, a straightforward diagonalisation of the effective Hamiltonian can be performed in the limit of high saturation. Here the kinetic terms and the radiative decay are removed and later been treated with the perturbation theory. One gets the following eigenvalues; $\lambda = 0$, $\lambda = \pm 1/2$, and $\lambda = \pm\sqrt{3}/2$ (in units of $\hbar\Omega$), with the eigenstates

$$\begin{aligned} |\lambda = 0\rangle &= \frac{1}{\sqrt{3}}\left(\,|{\rm g}\,;q-2\hbar k\rangle - |{\rm g}\,;q\rangle + \right. \\ &+ \left. |{\rm g}\,;q+2\hbar k\rangle\,\right) \qquad (6) \\ |\lambda = \pm 1/2\rangle &= \frac{1}{2}\left(-\,|{\rm g}\,;q-2\hbar k\rangle \mp |{\rm e}\,;q-\hbar k\rangle \pm \right. \\ &\pm \left. |{\rm e}\,;q+\hbar k\rangle + |{\rm g}\,;q+2\hbar k\rangle\,\right) \qquad (7) \\ |\lambda = \pm\sqrt{3}/2\rangle &= \frac{1}{\sqrt{12}}\Big(\,|{\rm g}\,;q-2\hbar k\rangle \pm \sqrt{3}\,|{\rm e}\,;q-\hbar k\rangle + \\ &+ 2\,|{\rm g}\,;q\rangle \pm \sqrt{3}\,|{\rm e}\,;q+\hbar k\rangle + \\ &+ |{\rm g}\,;q+2\hbar k\rangle\,\Big)\,. \qquad (8) \end{aligned}$$

In this context the $|\lambda = 0\rangle$ state has any excited state component with three peaks at $p = 0$ and $p = \pm\,2\hbar k$, thus very similar to the example shown in fig. 7c. The $|\lambda = 0\rangle$ state gets a finite lifetime firstly due to the kinetic term which mix it to the $|\lambda = \pm 1/2\rangle$ and $|\lambda = \pm 3/2\rangle$ states and secondly due to the off-resonant coupling to the $|{\rm e}\,;q \pm 3\hbar k\rangle$

states. Using perturbation theory, the imaginary part, of the $|\lambda = 0\rangle$ state can be calculated. With $q \ll \hbar k$, one gets:

$$\Gamma_{\lambda=0} = \Gamma_{\rm kin} + \Gamma_{\rm off}\,, \tag{9}$$

where

$$\begin{aligned}\Gamma_{\rm kin} &= -\frac{(8\omega_{\rm r})^2}{27}\frac{4\Gamma}{\Omega^2}\left(1+9\left(\frac{q}{\hbar k}\right)^2\right)\\ \Gamma_{\rm off} &= -\frac{\Gamma\Omega^2}{3}\frac{1}{2(5\omega_{\rm r})^2+\Omega^2}\\ &\times \left(1+\frac{(40\omega_r^2)^2}{(2(5\omega_{\rm r})^2+\Omega^2)^2}\left(\frac{q}{\hbar k}\right)^2\right).\end{aligned} \tag{10}$$

The general dependance of $\Gamma_{\lambda=0}$ at $q = 0$, given by relation 9, is fund to be in good agreement with the numerical simulation presented in fig. 7. Moreover, the q dependence of $\Gamma_{\lambda=0}$ indicates that the long lived state is also velocity selective. This point is particularly important for a VSCPT cooling scheme.

Momentum distributions corresponding to the $|\lambda = 0\rangle$ state have also been observed in the experiment, as shown in fig. 6. The detailed VSCPT distribution is shown as a residual, where the slow varying envelop has been numerically removed. We observe three peaks of the same height in good agreement with the prediction from fig. 7c. However the measured intensity is $I \approx 130 I_{\rm sat}$, *i.e.*, $\Omega \approx 12\omega_{\rm r}$. Even if the $|\lambda = 0\rangle$ state is still a long-lived one at this value, the intensity is two times larger than the predicted optimum one ($\Omega \approx 4.5\omega_{\rm r}$). This discrepancy may be due to an absence, in our simplified model, of a dynamical description of the population of the long-lived state. Indeed the model gives a prediction of the escape rate via the state lifetime but the feeding process is not described. The observation of those long lived states may occur at a larger or shifted range of intensity than the model prediction. Indeed only smooth changes, as function of the system parameter, on the multi peak structure have been observed so far. Moroever, since the image of fig. 6 does not reveal any peaks at $\pm 3\hbar k$, the $\pm\hbar k$ structure can still be associated to the state $(|{\rm g}\,;-\hbar k\rangle - |{\rm g}\,;+\hbar k\rangle)/\sqrt{2}$, corresponding to the low intensity case.

Conclusions. – VSCPT-cooling on a two-level atomic system has been experimentally demonstrated. This is possible, since the atomic transition used, in Sr, has a narrow linewidth, making the otherwise open family of momentum states, $|{\rm g}\,;-\hbar k\rangle$, $|{\rm e}\,;0\rangle$, and $|{\rm g}\,;+\hbar k\rangle$, less open, due to kinetic detuning from other momentum states. Thus, a semi-dark state is formed. During the cooling, the long-lived state, of sub-recoil width, is fed with atoms, while there is simultaneously a constant loss. For a favourable ratio between the feeding rate and the loss rate, the momentum profile acquires narrow peaks, centered at $\pm\hbar k$, that lie on top of the Doppler cooled profile. At best, the steady-state population of the dark state reaches $\approx 10\%$.

At high saturation, complex momentum profiles arise with subrecoil peaks also resulting from a coherent population trapping mechanism. With an analysis based on an effective Hamiltonian approach, we have identified the observed multipeak structures to long lived states.

* * *

Freddy Bouchet, Claude Dion and Mats Nylén are kindly acknowledged for discussions. A.K. thanks the *International Cold Atom Network (INTERCAN)* for support, and the staff at INLN for hospitality. This work was financially support by the *Conseil général des Alpes-Maritimes* and the *Laboratoire National de Métrologie et d'Essai (LNE)*.

REFERENCES

[1] Zibrov A. S., Lukin M. D., Nikonov D. E., Hollberg L., Scully M. O., Velichansky V. L. and Robinson H. G., *Phys. Rev. Lett.* , **75** (1995) 1499.
[2] Anderson B. P. and Kasevich M. A., *Science* , **282** (1998) 1686.
[3] Peters A., Chung K. Y. and Chu S., *Metrologia* , **38** (2001) 25.
[4] Alzetta G., Gozzini A., Moi L. and Orriols G., *Nuovo Cimento B* , **36** (1976) 5.
[5] Aspect A., Arimondo E., Kaiser R., Vansteenkiste N. and Cohen-Tannoudji C., *Phys. Rev. Lett.* , **61** (1988) 826.
[6] Lawall J., Bardou F., Saubamea B., Shimizu K., Leduc M., Aspect A. and Cohen-Tannoudji C., *Phys. Rev. Lett.* , **73** (1994) 1915.
[7] Lawall J., Kulin S., Saubamea B., Bigelow N., Leduc M. and Cohen-Tannoudji C., *Phys. Rev. Lett.* , **75** (1995) 4194.
[8] Saubamea B., Hijmans T. W., Kulin S., Rasel E., Peik E., Leduc M. and Cohen-Tannoudji C., *Phys. Rev. Lett.* , **79** (1997) 3146.
[9] Olshanii M. A. and Minogin V. G., *Opt. Commun* , **89** (1992) 393.
[10] Prudnikov O. N. and Arimondo E., *J. Opt. Soc. Am. B* , **20** (2003) 909.
[11] M. T. Widmer, M. R. Doery, M. J. Bellanca, W. F. Buell, T. H. Bergeman, and H. J. Metcalf, *Phys. Rev. A* , **53** (1996) 946.
[12] Doery M. R., Vredenbregt E. J. D. and Bergeman T., *Phys. Rev. A* , **51** (1995) 4881.
[13] Hack J., Liu L., Olshanii M. and Metcalf H., *Phys. Rev. A* , **62** (2000) 013405.
[14] Chanelière T., Meunier J.-L., Kaiser R., Miniatura C. and Wilkowski D., *J. Opt. Soc. Am. B* , **22** (2005) 1819.
[15] Chanelière T., He L., Kaiser R. and Wilkowski D., *Eur. Phys. J. D* , **46** (2008) 507.
[16] Castin Y., Wallis H. and Dalibard J., *J. Opt. Soc. Am. B* , **6** (1989) 2046.